RESEARCH ARTICLE

Recent Advances in Large Area Silicon Avalanche Photodiodes for Particle Detection

Michael R. Squillante[1], James F. Christian[2], Mickel McClish[3]

Authors' Affiliation:

Radiation Monitoring Devices, Inc., 44 Hunt St., Watertown, MA 02451

Authors e-mail address:

[1] **Corresponding author:** MSquillante@RMDInc.com

[2] JChristian@RMDInc.com

[3] MMcClish@RMDInc.com

Abstract

This work presents advancements in silicon large-area avalanche photodiodes (LA-APD) for use as charged-particle and photo-detectors with internal gain when operated at a sufficiently high bias. Improvements in wafer processing, innovative surface fabrication techniques, and specialized electrode configurations has led to the production of hyper-fast APD devices with picosecond timing capability. In addition, APD photosensors with high quantum efficiency in the ultraviolet (UV) have been produced, which have the ability to discriminate the UV photons from visible photons. LA-APDs can be fabricated as arrays and as position-sensitive detectors in sizes ranging from 2 mm^2 to over 160 mm^2.

1. Introduction

Avalanche photodiodes (APD) are silicon charged particle- and photo-detectors that are operated at a sufficiently high bias that electrons accelerate to a high enough energy to generate additional carriers by knock-on collisions with other electrons. This results in an internal signal gain, with an output that is linearly proportional to the detected signal. This linear response and internal gain make APDs unique devices that can provide a solution for challenging experimental measurements in physics for which no other detector technology is satisfactory. For gamma ray and charged particle detection, a photodetector is coupled to a scintillation material, however, APDs can directly detect x-rays and charged particles.

Despite advances in readout electronics, the small signal performance of photodiodes is often limited by noise in the preamplifier used to amplify the signal. One method to overcome this problem is to design a device with internal gain, like the APDs. In its simplest form, an APD is a p-n junction

formed in a silicon wafer, structured so that it is operated near breakdown voltage under reverse bias. Compared to conventional photodiodes, relatively large output pulses are produced along with an improved signal-to-noise ratio [1-9], where the internal gain reduces the relative effect of the noise associated with the readout electronics.

APDs can be fabricated as single element photodiodes, pixelated arrays, and position-sensitive devices, PS-APD [10]. The arrays and PS-APDs are used in preclinical nuclear medicine imaging systems for research. As is the case with the Anger-like readout approach, the PS-APD can perform imaging with many fewer readout channels than pixelated devices.

LA-APDs were initially investigated for use as fast, large-area optical sensors, however, they are also sensitive to directly incident ionizing radiation, including X-rays, alpha particles, and beta particles [8]. The high signal-to-noise ratio due to the silicon Fano factor and internal gain makes them particularly useful for detecting low energy radiation at room temperature. APDs can also be used to detect low energy X-rays, such as the 5.9 keV X-rays from ^{55}Fe. At 5.9 keV, an energy resolution of 550 eV is achievable for 9 × 9 mm^2 APDs at room temperature. The noise level in APDs can be as low as about 200 eV for devices with an active area of less than about 5 mm^2 and with sufficient cooling, the resolution can be lowered further. APDs are useful for detecting X-rays in the range of about 1 keV, to about 20 keV, limited by the X-ray stopping power of silicon.

One key advantage of silicon APDs is that they can detect charged particles through direct interactions with the silicon. This article reviews APD technology and describes recent advances in APDs particularly in the context of applications that capitalize on the unique performance attributes of silicon APDs.

An example of projects where fast APD particle detectors could offer enhanced performance are the new generation of large very intense colliders, such as the Large Hadron Collider (LHC). As the luminosity increases, the event rate increases. Increasing the luminosity will allow science to move from exploration to precision studies and this requires detector technologies that go beyond what is currently being used. One of the improvements currently being sought are detectors with improved timing resolution for direct particle detection that can process events at high event rates.

Another capability of APD's is their ability to provide monolithic position-sensitive devices, which is particularly advantageous when detecting and locating charged particles through direct interactions. (For example, beam monitors for accelerators and "telescope" configurations for particle identification in space applications.)

2. Hyperfast APD Photosensors

Some experiments require much faster response, especially experiments planned for the next generation of high intensities of minimum ionizing particles (MIPs), such as the Large Hadron Collider (LHC). To go beyond the limits of APD capabilities, alternative device structures and readout approaches are needed. We demonstrated that excellent timing performance can be achieved by making use of the mirror charge produced at the p-side charge

carriers; combining this with an innovative electrode structure, further improved timing to below 10 ps RMS (Root Mean Square) for optical detection [11,12]. This was achieved by reducing the APD series resistance using a conductive fine mesh screen onto the APD p-side anode sensing surface and by using sintered gold to form a large-area cathode electrode (to lower the series resistance and improve the APD electric field uniformity). Signal response uniformity was measured by using optical equivalent MIP signals with X-Y scans (using the Transient Current Technique (TCT)). Signals from the mesh APD were processed using a fast bench top signal digitizer.

2.1. Fabrication of Gold Sintered APDs

To lower the contact resistance, and thus the overall APD series resistance, we created a different cathode electrode from what we use to fabricate our standard APDs by attaching a conductive mesh screen on top of cathode sensing surface. A high dielectric film (Kapton) is placed between the screen and the cathode surface. When combined with a gold sintered electrode deposited on top of the standard n+ electrode, the induced signal from the screen offered a reduced signal time walk and time jitter, and improved the signal amplitude uniformity compared to standard APDs.

To create the gold electrodes, we used a solid metal evaporation mask placed on the n-side of the silicon wafer. When fabricating multiple 9 × 9 mm^2 APDs within a wafer, the mask was fabricated to have a pattern of 7 × 7 mm^2 square cutouts that matched the location and area of the n-side electrodes for each APD. Gold was then evaporated onto the silicon wafer into regions not covered by the mask creating a gold layer on the square n+ electrodes that was approximately 100 nm thick. This is followed by heating the wafer (370 to 380 °C for 5 minutes) to sinter the gold. Figure 1 shows a photograph of the n-side of several APDs produced in this way. The metalized anode is nearly the same area as the chip. The black colored area is the portion of the n-side covered by a passivation polyimide coating. Some of these chips went on to be coupled to mesh screens and packaged at Radiation Monitoring Devices, Inc., Watertown, MA (RMD).

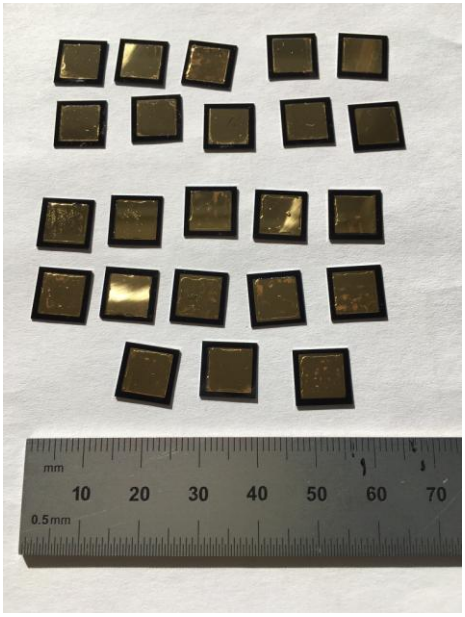

Figure 1. A photograph showing 9×9 mm^2 APDs fabricated with a gold sintered n+ electrode.

Figure 2 is a diagram showing the cross-sectional view and dimensions of packaged mesh APDs. A thin conformal coating was used to adhere to the Kapton film and mesh screen together on the APD surface at the cathode, which is faced up in Figure 2. In

this configuration, the mesh APD is biased with a negative high-voltage applied to the cathode and the anode to ground. The mesh screen, which produces the induced mirror charge signal, is electrically floating. This packaging approach allows the mesh APDs to be easily handled and easily connected to any readout circuitry for the laboratory evaluations described below.

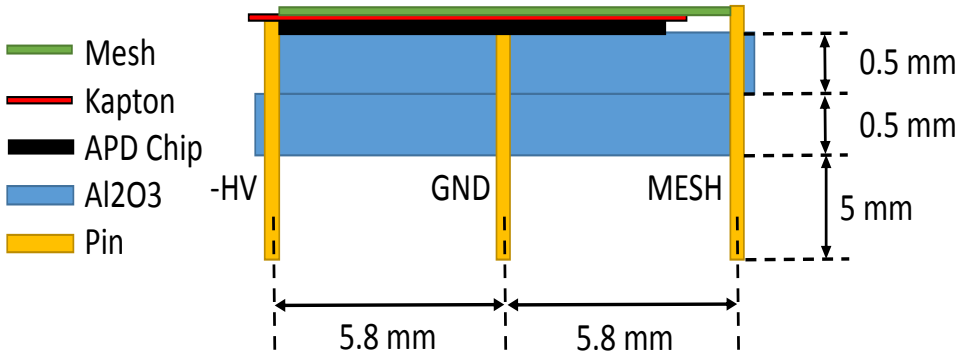

Figure 2. A diagram showing the cross-sectional view of packaged 9 × 9 mm^2 mesh APDs. (Not drawn to scale.)

2.2. Evaluating Mesh electrode APDs

Square 9 × 9 mm^2 APDs with mesh electrodes were evaluated for their gain and dark noise characteristics at RMD. The gain measurement involved recording the amplitude of the mesh APD anode signal when illuminated with a pulsed unfocused red LED light source. Initial measurements were conducted at low bias (500 V) to measure the pulse height corresponding to unity gain. The pulse height was recorded at higher bias settings to measure the relative gain versus bias relationship at various temperatures. Figure 3 shows the results gain vs. bias for different temperatures in the high-gain regime. These curves are reasonably typical for RMD's standard APD. By injecting test pulses into the preamplifier input, while simultaneously collecting ^{55}Fe (5.9 keV X-rays) spectra as an energy calibration, the full width at half maximum (FWHM) from a pulse generator (pulser) was used to quantify the noise. Mesh APDs at room temperature had 0.7 to 0.8 keV of noise, which is also reasonably typical for standard APDs (for the same area and testing conditions).

With the mesh APD gain *vs.* bias known for various temperatures, it is straightforward to then measure the detector dark current vs. gain at various temperatures. Figure 4 shows the measured dark current curves. Again, these values are typical for a standard 9 × 9 mm^2 APD and demonstrate that the configuration depicted in Figure 2 above does not increase the dark current of the device.

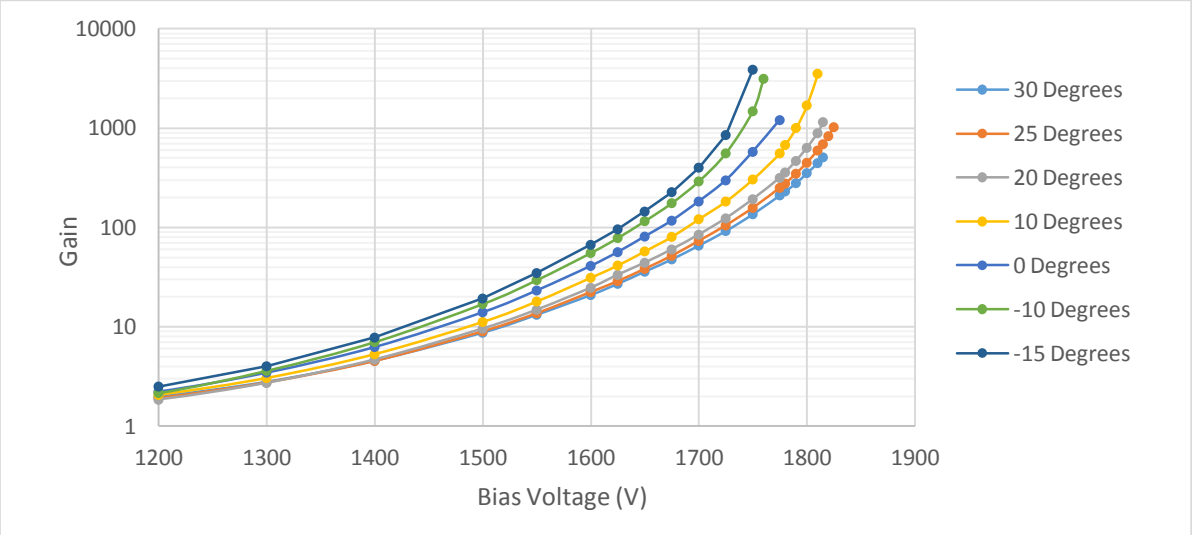

Figure 3. Gain vs. bias for various temperatures Celsius) for a mesh 9x9 mm^2 APD.

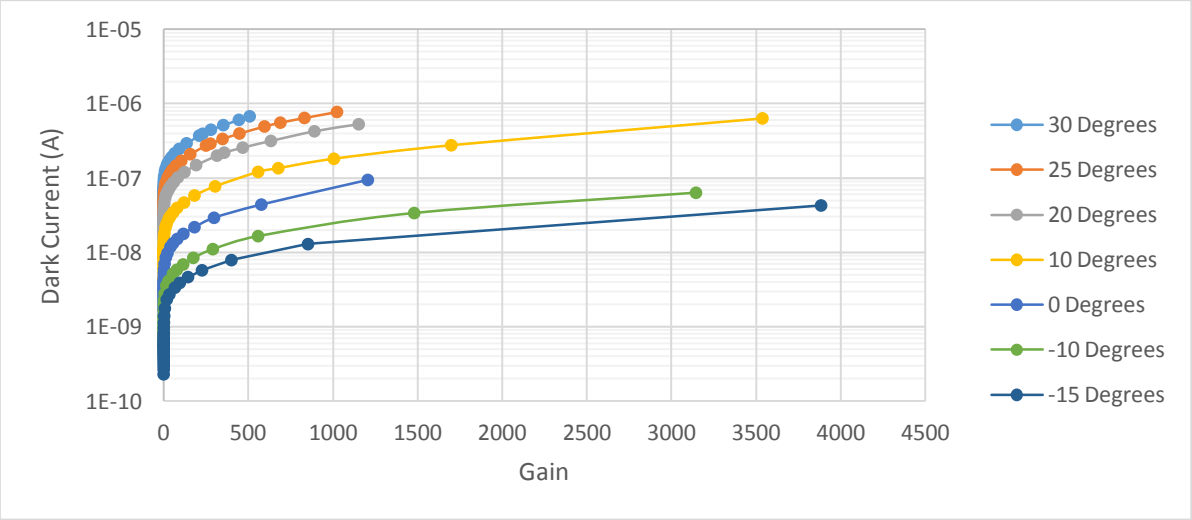

Figure 4. Mesh APD dark current vs. gain for various temperatures (in Celsius).

We also performed Transient Current Technique (TCT) X-Y scans of meshed APDs. The TCT records solid-state detector pulse shapes, from which the signal amplitude and signal timing properties can be monitored. The infrared (IR) light and the laser intensity were adjusted to produce minimum ionizing particle (MIP) equivalent signals. With the addition of an X-Y translation stage, the detector signals can be recorded as a function of position. In this way, a mesh APD was mounted with an operating bias applied, and scanned using a finely focused IR (1064 nm) pulsed laser. APD waveforms were captured by a fast digital oscilloscope by triggering the oscilloscope with the trigger output from the pulse generator (which triggers the IR laser diode). Figure 5 shows the TCT scan results from a small area on a mesh APD. The metallic screen is clearly visible as the color yellow, corresponding to a rise time of approximately 14 ns.

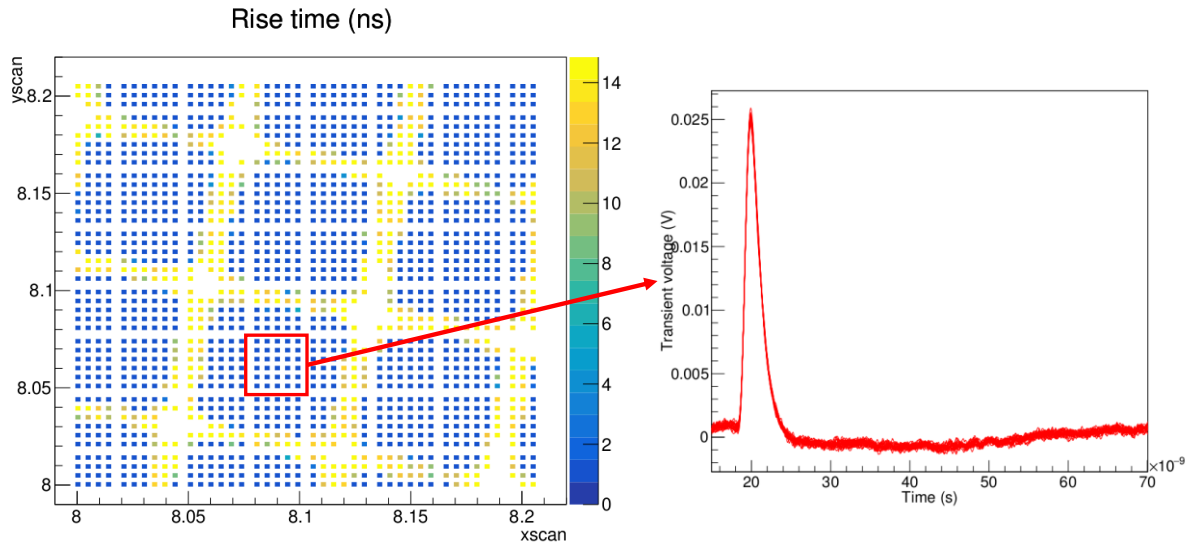

Figure 5. The TCT scan results for a small area on a mesh APD. The adjacent plot shows 30 TCT signals taken from the sample area boxed in the color red. The signals are very uniform in terms of rise time and amplitude.

Everywhere else, the rise time is much faster at approximately 1 ns and uniform. The 30 TCT signals in the red colored box area are all plotted in the adjacent plot. As can be seen, the signals are nearly identical in terms of rise time and amplitude.

We performed a series of optical timing resolution measurements using a 9 × 9 mm^2 mesh APD. A basic diagram of the measurement setup used is shown in Figure 6. A custom-made fast pulser, based on bipolar transistor breakdown, generated the short pulses. Its output was split in two parts by a passive splitter. One output of the splitter drove a 980 nm semiconductor laser diode, which provided short laser pulses sent through an optical fiber to the detector. The detector output signal was taken from the mesh induced signal and amplified by 50 dB before being digitized by SAMPIC. (The SAMpler for PICosecond time pick-off chip was developed by CEA Saclay and LAL Orsay, France for fast timing in particle physics or TOF-PET [16]). The second output of the splitter, attenuated by 10 dB, was sent to another channel on the SAMPIC chip.

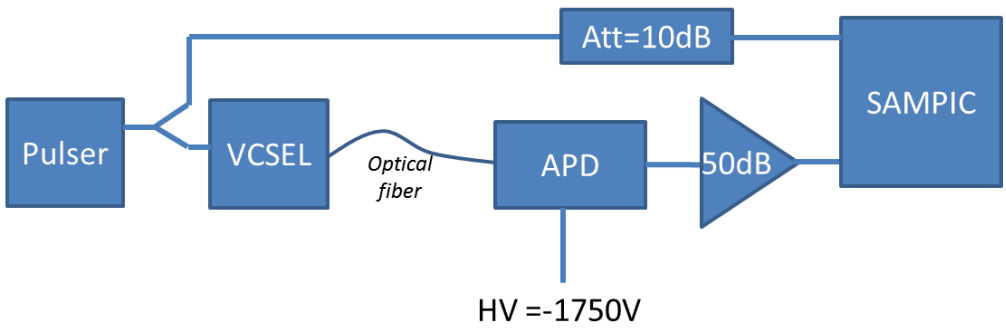

Figure 6. A basic diagram showing the mesh APD timing resolution test setup.

SAMPIC was used in self-trigger mode on both (independent) channels. A typical acquisition is shown in **Figure 7**. The detector pulse is delayed by ~12 ns with respect to the pulser signal. It is preceded by a perturbation (synchronous with the pulse). The amplitude of the digitized amplified detector signal is ~ 650 mV with a rise time of ~1.3 ns. The timing of both pulses has been extracted using a digital CFD (dCFD) algorithm with a fraction of 0.6. The distribution of the time differences between the two pulses for 50k events is shown in Figure 8, along with a Gaussian fit (red) having σ = 12 ps RMS.

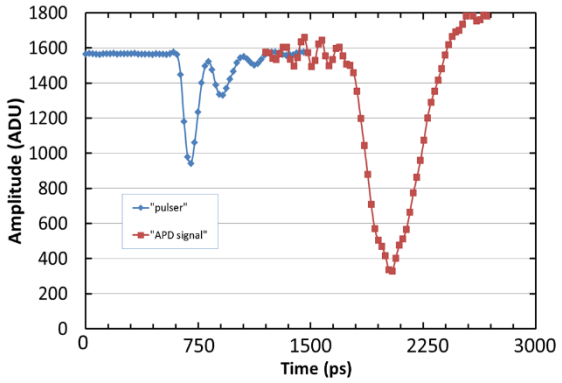

Figure 7. A plot showing the mesh APD and pulser signal digitized by SAMPIC.

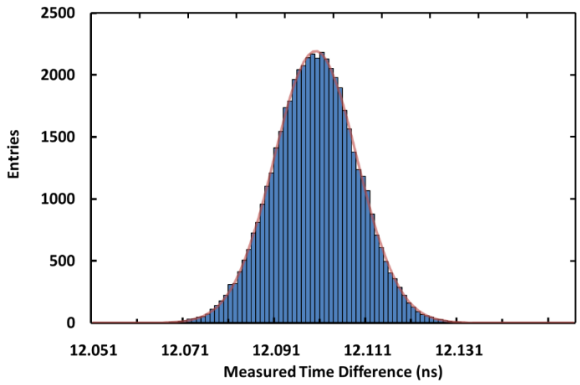

Figure 8. Distribution of the arrival time difference between the pulser and detector signals. The red trace is the Gaussian fit. The standard deviation is 12 ps RMS.

3. Calorimeters using fast APDs as photodetectors.

Another example where the unique properties of APDs provide a performance benefit is in the detection of UV scintillations from crystals, like BaF_2, used in particle calorimeters. Fast efficient detection in the UV is challenging, and even more so if detection of photons in the visible region of the spectrum must be avoided. Researchers involved in the search for new high energy particles need fast detectors and calorimeters. BaF_2 has very high particle and photon stopping power and a very fast UV emission, about 900 ps at 220 nm, but also has an emission at 310 nm with a very long decay time of approximately 650 ns. To take full advantage of the fast response of BaF_2, a fast photodiode that detects the 220 nm emission is needed, but which can also ignore the slower 330 nm emission. To address this need, research was undertaken to improve both the far UV sensitivity and reduce sensitivity at longer wavelengths. Improvements in UV sensitivity were coupled with research to improve speed of response.

Because UV photons do not penetrate deeply into silicon, the sensitivity of any silicon device is limited by the collection of the charge carriers near the surface of the device. All semiconductor photodetectors have a “dead layer” near the front surface

caused by defects and surface states, where charge transport and charge collection are poor. To improve the APD UV sensitivity, the active layer of the APD must approach the surface. Typically, the front surface passivation process creates a dead p+ layer of about 100 nm thick. At 220 nm, the photon penetration depth in silicon is < 10 nm. A thinner p+ surface layer, with an appropriate p-type dopant concentration, reduces UV absorption in this layer and reduces charge carrier losses at the sensing surface from trapping and recombination. This was accomplished using molecular beam epitaxy, MBE, to create a 5-nm thick, superlattice structure with a well-defined, highly doped p+ passivation layer [13-16].

Before the superlattice structure was grown, APDs were thinned on the p-side to decrease the thickness of the neutral drift region, where charge transport is slow due to a weak electric field. With a thinner neutral drift region, the UV generated photoelectrons will more quickly reach the avalanche region (where the electric field is very high), improving the APD response time, and with fewer photoelectrons lost to recombination during the transit through the drift region to the avalanche region, thereby increasing the quantum efficiency. Figure 9 shows the cross section drawings for RMD's standard APD and the superlattice-doped APD (SL-APD). Devices with two layer or four layer superlattices were fabricated and studied.

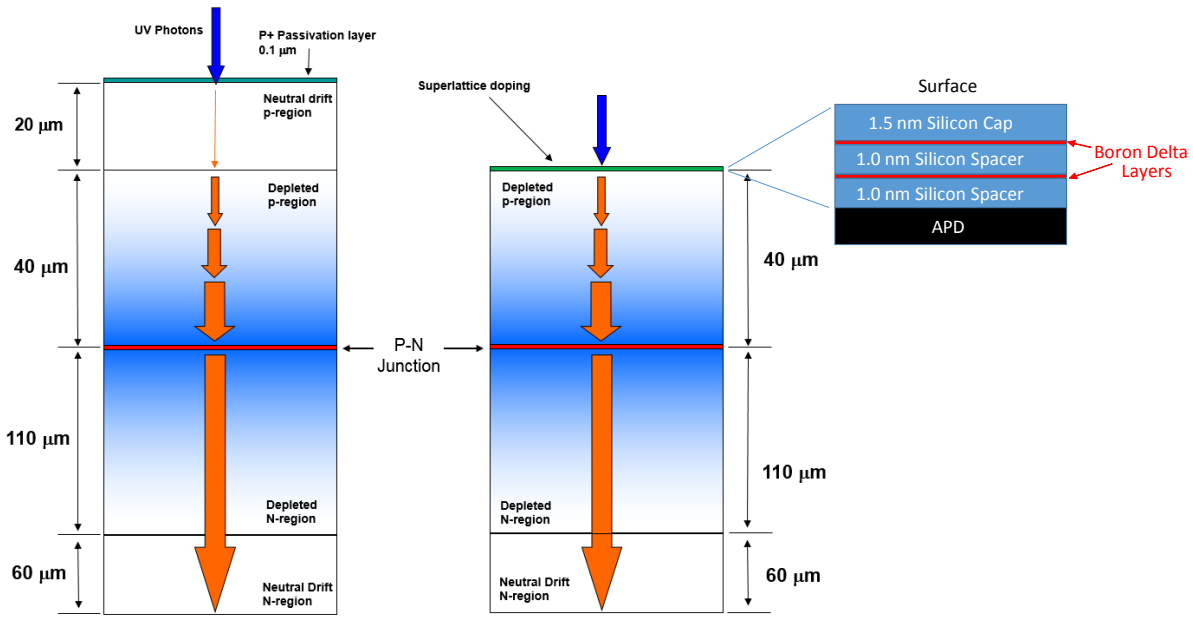

Figure 9. An APD cross-sectional view, not drawn to scale, showing the various p and n regions when the APD is biased. The standard APD is on the **left** and the SL-APD is on the **right**. Also shown is a close up view of a 2-layer MBE structure. Included is a visualization of the photocurrent generation process in orange.

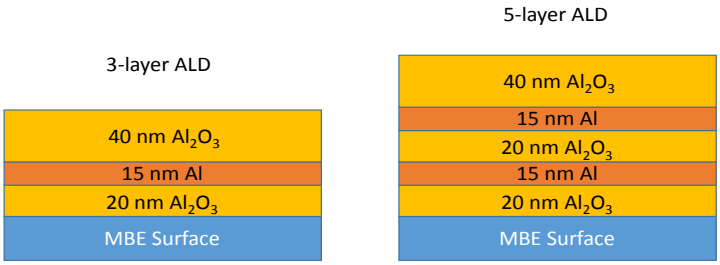

Figure 10. A drawing depicting the 3 and 5-layer ALD Al_2O_3/Al passband filters.

To detect the transmission of the fast emission from BaF_2 at 220 nm while attenuating the slower, longer wavelength component, a specific passband filter was modeled and engineered. The filter was comprised of alternating layers of Al_2O_3 and Al on the MBE top surface grown using an atomic layer deposition (ALD) process. We explored two different filters, one comprised of three layers and the other with five layers. Figure 10 shows a cross sectional view of the two types of ALD grown passband filters. As will be shown below, the three layer filter, while offering a high transmission at 220 nm, also allows some out-of-band light to leak through. The five layer filter, conversely, lowers the transmission at 220 nm, but also more strongly attenuates any out-of-band light.

This basic packaging scheme functioned well and allowed for easy handling of individual APDs for testing. Figure 11 shows a photograph of two packaged 9 × 9 mm^2 SL-APDs with an ALD filter coating.

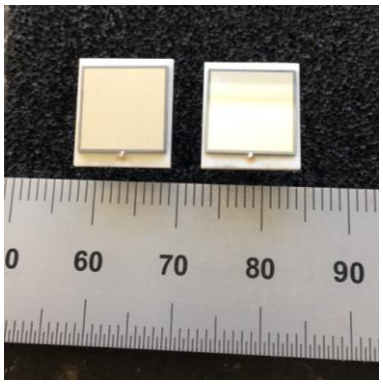

Figure 11. Photo of two 9 × 9 mm^2 SL-APDs with the ALD filter.

3.1. Superlattice APD Characteristics

We performed evaluations of the various SL-APD. Gain was determined by measuring the output signal when illuminated with a pulsed unfocused LED light source. The initial measurement was conducted at 500 V (unity gain). The pulse height was then recorded at higher bias values to compute the relative gain versus bias relationship. We performed the gain measurement using 400-nm light (< 1 μm penetration depth). An SL-APD can achieve relatively high gain. The gain vs. bias behavior is similar to that which is typically observed with RMD's standard APD. At 1780 V bias, the SL-APD gain was approximately 450.

Electronic Noise in the SL-APD was measured with the APDs under biased while pulse height data were recorded from incident low energy X-rays (5.9 keV) while simultaneously injecting an electronic test pulse into the preamplifier input via a 1 pF capacitor. The preamplifier output signal was shaped using a 0.25 μsec shaping time. The 5.9 keV X-ray peak was used to calibrate the energy scale. Test pulse peak broadening, recorded on the calibrated scale, provided an estimation of the relative APD total electronic noise. As the gain (bias) is increased, the signal-to-noise ratio decreases to a minimum and then begins to rise due to the increasing dark current, which is the dominant noise source. This noise vs. gain behavior is typical for RMD APDs, however, the SL-APD has greater noise than a standard APD. The source of the excess dark current has not been clearly identified. We have been able to determine that the increased dark current is not due to the passband filter. The higher dark current appears to be related to the boron concentration in the MBE layers, as well as how the MBE surface is prepared for the passband filter growth.

Quantum efficiency was measured from 200 nm to 500 nm. Figure 12 shows the results for three 9 × 9 mm^2 SL-APDs having a 3-layer, a 5-layer standard filter, and no filter. A standard APD is shown as well. The external QE for the 5-layer and 3-layer SL-APD reached 31% and 50% at 220 nm, respectively. This demonstrates how, and how well, the passband filters work when compared to the QE of an uncoated SL-APDs and a standard device.

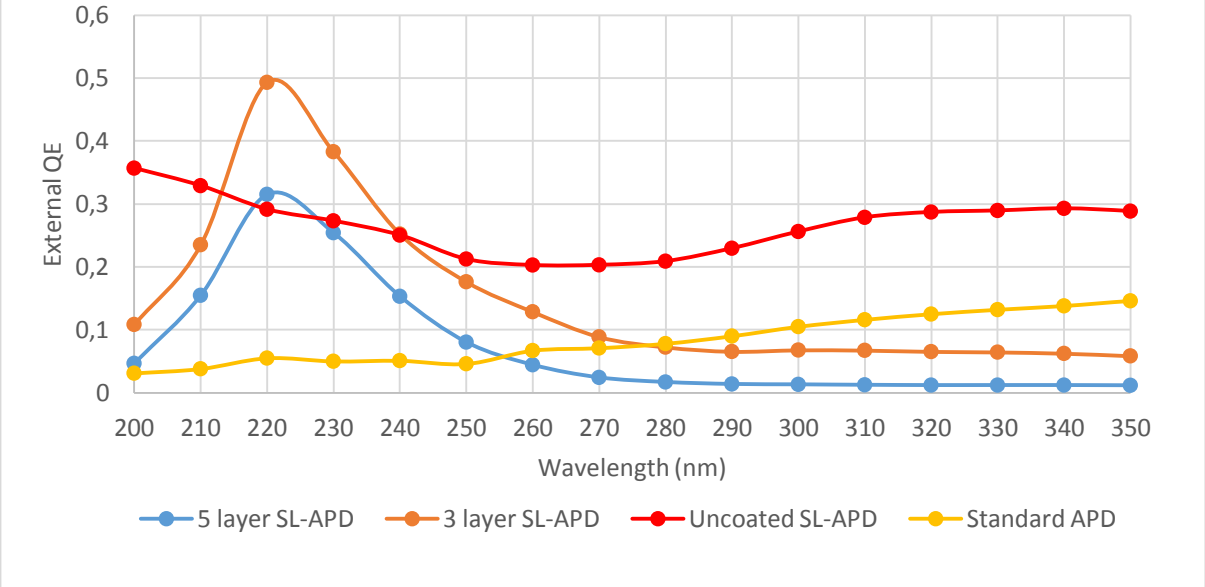

Figure 12. A plot showing the external QE for a 9 × 9 mm^2 SL-APD coated with 3-layer and 5-layer of ALD Al_2O_3/Al passband filters and an uncoated SL-APD (red). A standard APD is shown as well (yellow).

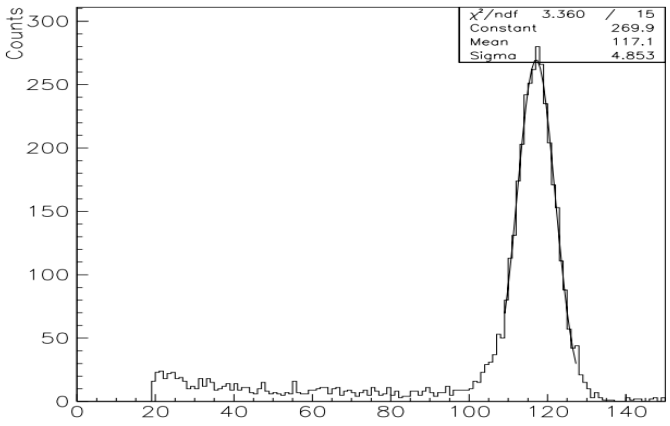

Figure 13. Energy spectrum obtained from scintillations produced in liquid xenon by 5.5 MeV alpha articles.

4. APDs for Dark Matter detection

Fast, UV sensitive large area avalanche photodiodes can be used in the search for dark matter. The high sensitivity to far-UV photons makes it possible to detect scintillation pulses in liquid xenon (178 nm) and liquid argon (124 nm). Figure 13 shows an alpha particle spectrum taken with an APD immersed in liquid xenon as the photodetector for the ultraviolet scintillation light of liquid xenon (LXe) whose temperature is between 167 K and 188 K [17, 18]. As a consequence of the low temperatures of LXe, the APD can greatly benefit from the cold conditions to lower the dark noise and increase the gain (for a given bias). This also affords the use of larger area APDs, which could otherwise have prohibitive amounts of dark current at room temperature. So, the high quantum efficiency and high gain of the APD make it an attractive alternative UV photosensor to PMTs for LXe detectors for dark matter experiments.

5. Summary

Recently there have been significant technical breakthroughs in fabricating large-area APDs, APD arrays, and position sensitive APDs (PSAPDs) for use in particle detection experiments as both direct particle detectors and as scintillation detectors. When used as a charged particle detector, APDs provide the unique capability of converting energy deposited into electron-hole pair signal with sub-Poisson statistics, as described by the Fano factor. This provides a unique advantage over comparable scintillation detection configurations. In physics experiments where very high event rates are encountered, and for other demanding applications where no existing device is suitable, APDs might provide the solution.

Acknowledgements

The authors gratefully acknowledge the support for portions on this research from the U.S. Department of Energy under SBIR Grant No. DE-SC0011316, “Superlattice Doped Avalanche Photodiodes for Improved UV Sensitivity in Scintillator Calorimetry, and Grant No. DE-SC0015938 “Hyperfast Silicon Detector for Direct Particle Detection”.

References

[1] G.C. Huth, "Recent results obtained with high internally amplifying semiconductor radiation detectors", *IEEE Trans. Nucl. Sci*. NS-13(1) 36 (1966)

[2] Reiff, G.; Squillante, M.R.; Serreze, H.B.; Entine, G.; and Huth, G. Large Area Silicon Avalanche Photodiodes: Photomultiplier Tube Alternate. Materials Research Society Symposium Proceedings 16 Nuclear Radiation Detector Materials:131-140, 1983.

[3] Entine, G.; Reiff, G.; Squillante, M.R.; Serreze, H.B.; Lis, S.; and Huth, G. Scintillation Detectors Using Large Area Silicon Avalanche Photodiodes. IEEE Transactions on Nuclear Science NS-30(1):431-435, 1983.

[4] Olschner, F.; Farrell, R.; and Squillante, M.R. *New Technology for Room Temperature Silicon X-ray Detectors*. Invited presentation at the 29th Meeting of the Microbeam Analysis Society, Breckenridge, CO, 1995.

[5] Farrell, R.; Vanderpuye, K.; Cirignano, L.; Squillante, M.R.; and Entine, G. *Radiation Detection Performance of Very High Gain Avalanche Photodiodes*. Nuclear Instruments & Methods in Physics Research **A353**:176-179, 1994.

[6] Squillante, M.; Gordon, J.S.; Farrell, R.; Vasile, S.; Daley, K.; Oakes, C.; and Vanderpuye, K. *Recent Advances in Avalanche Photodiode*

[7] Vasile, S.; Gordon, J.S.; Farrell, R.; and Squillante, M.R. *Fast Avalanche Photodiode Detectors for the Superconducting Super Collider*. Mat. Res. Soc. Symp. ProcMonitoring Low Levels of Tritium. Fusion Technology, September 1988.

[8] Squillante, M.R.; Farrell, R.; Lund, J.C.; Sinclair, F.; Entine, G.; and Keller, K.R. Avalanche Diode Low Energy X-ray and Nuclear Particle Detector". IEEE Transactions on Nuclear Science, vol. 33, issue 1, pp. 336-339 (1986) DOI: 10.1109/TNS.1986.4337113

[9] J. Campbell, Chapter 8, "Advances in Photodetectors", in Optical Fiber Telecommunications VA, 5th Edition, Components and Subsystems, Academic Press, Ivan Kaminow Tingye Li Alan E Willner Editors, 2008

[10] K.S. Shah, et al., "Large Area APDs and Monolithic APD Arrays," *IEEE Trans. Nucl. Sci.*, vol. 48, no. 6, p. 2352 (2001).

[11] M. Centis Vignali, ,M. Gallinaro, , B. Harrop, C. Lu, M. McClish, K. T. McDonald, M. Moll, F. M. Newcomer, S. Otero Ugobono, and S. White, "Characterization of Irradiated APDs for Timing Applications", 31st RD50 workshop, CERN 11/21/2017.

[12] M. Centis Vignal,R. Dalal, B. Harrop, G. Jain, C. Lu, M. McClish, K. T.

McDonald, M. Moll, F. M. Newcomer, S. Otero Ugobono, and S. White, "Study of Deep Diffused APDs for Timing Applications", 06.06.2017 30th RD50 workshop, Krakow, 6/6/2016

[13] M. E. Hoenk, A. G. Carver, T. Jones, M. Dickie, P. Cheng, F. Greer, S. Nikzad, J. Sgro, S. Tsur, "The DUV Stability of Superlattice-doped CMOS Detector Arrays," Proceedings of the 2013 International Image Sensor Workshop, Snowbird, UT, June 12-16, 2013.

[14] Hoenk, M.E., A.G. Carver, T.J. Jones, M. Dickie, S. Nikzad, J. Sgro, S. Tsur, "Superlattice-doped Imaging Detectors: Structure, Physics, and Performance," Proceedings of the Scientific Detectors Workshop, Florence, Italy, October 7-11, 2013.

[15] M. E. Hoenk, S. Nikzad, A. G. Carver, T. J. Jones, J. Hennessy, A. D. Jewell, J. Sgro, S. Tsur, M. McClish, R. Farrell, "Superlattice-doped imaging detectors: progress and prospects," *Proc. SPIE*. 9154, High Energy, Optical, and Infrared Detectors for Astronomy VI, 915413. 2014.

[16] M. E. Hoenk, "Surface Passivation by Quantum Exclusion Using Multiple Layers," U.S. Patent 8,395,243, issued March 12, 2013.

[17] P. Shagin, R. Gomez, U. Oberlack, P. Cushman, B. Sherwood, M. McClish, R Farrell, Avalanche photodiode for liquid xenon scintillation: quantum efficiency and gain, JINST 4 (2009) 1005

[18] V.N Solovov, A Hitachi, V Chepel, M.I Lopes, R.Ferreira Marques, A.J.P.L Policarpo, ," Detection of scintillation light of liquid xenon with a LAAPD", In Volume 488, Issue 3, 2002, Pages 572-578, ISSN 0168-9002, https://doi.org/10.1016/S0168-9002(02)00517

